RSC Advances

ROYAL SOCIETY OF CHEMISTRY

www.rsc.org/advances

Journal Name

RSCPublishing

ARTICLE

Effect of metal content in the electrocatalytic activity of Au_xPd_y mixtures and their use in a glucose membraneless microfluidic fuel cell

Cite this: DOI: 10.1039/x0xx00000x

Received ooth January 2012,
Accepted ooth January 2012

DOI: 10.1039/x0xx00000x

www.rsc.org/

N. Arjona,[a] A. Dector,[a] M. Guerra-Bálcazar,[b] L. Álvarez-Contreras,[c] N. Sabaté,[d] J. P. Esquivel,[d] J. Ledesma-García,[c+] and L. G. Arriaga[a*]

Au_xPd_y bimetallic mixtures with different elemental contents were synthesized on glassy carbon electrodes using electrochemical techniques which are easy, quick, versatile and cheap. Pulse potential and staircase techniques such as cyclic voltammetry ($Au_{60}Pd_{40}$), square wave voltammetry ($Au_{50}Pd_{50}$ and $Au_{35}Pd_{65}$) and second harmonic AC voltammetry ($Au_{15}Pd_{85}$) were used to easily change the metal proportion and reduce the Au content in the Au_xPd_y mixtures. $Au_{60}Pd_{40}$ exhibited the most negative potential (-0.4 V vs. NHE) toward the glucose electrooxidation reaction. For this reason was then synthesized in the anode compartment of a microfluidic fuel cell and compared with single Au and Pd synthesised also by cyclic voltammetry. $Au_{60}Pd_{40}$ showed a more negative potential than the Au anode; meanwhile Pd showed no electrocatalytic activity. The lattice parameters were calculated by X-Ray Diffraction patterns resulting in values of 3.83 and 4.03 Å for Au and Pd, respectively and 3.94 Å for $Au_{60}Pd_{40}$ evidencing internal structural changes due to the incorporation of Pd to the Au matrix. The maximum power density obtained with a glucose membraneless microfluidic fuel cell GMMFC using 10 mM glucose and $Au_{60}Pd_{40}$ as anode was of 0.28 mW cm^{-2}.

Introduction

Research in microfluidic fuel cells utilizing glucose as fuel has shown a growth in the last few years.[1-3] The main reason is related with its easy production and handling; besides has shown intuitive application for implantable and portable fuel cell applications.[4] In this context, microfluidic fuel cells are a kind of fuel cells that operates without a membrane to separate the anode and cathode.[5] A natural interface between fuel and oxidant is formed due to the laminar flow regimen produced when they are introduced in a microchannel, allowing independent electrochemical reactions in each stream.[6]

Different catalytic materials have been evaluated in the glucose microfluidic fuel cells, such as modified or immobilized enzymes,[7-10] noble metals like gold supported on vulcan carbon or multi-walled carbon nanotubes.[3, 11, 12] The AuPd mixture has been reported using different chemical synthesis methods. Some of the reported pathways are via chemical reduction method,[13] thermal chemical vapour deposition,[14] the reversible addition-fragmentation chain transfer (RAFT) polymerization,[15] and electrodeposition using differential pulse amperometry.[16] The AuPd mixture has been used for the electrooxidation of formic acid,[13] glycerol,[17] and carbon monoxide;[18] the hydrogen evolution reaction,[19] and hydrogen peroxide electroreduction.[16]

The effect of Au and Pd molar content in AuPd materials toward the glucose electrooxidation reaction has been recently investigated by Yan et al.[20] They found that introducing Au to the Pd lattice allowed increasing the tolerance to glucose by-products. Zhang et al,[13] as well as Park et al,[21] also observed that the electrocatalytic properties of AuPd are enhanced in terms of the stability (decreasing the CO poisoning) and activity for the formic acid electrooxidation reaction.

The miniaturization of membraneless fuel cells involves the decrease of the electrode size and hence, increases the difficulty for the electrocatalysts incorporation in the electrode surface. Electrodeposition is an easy, cheap, quick and versatile synthesis method. The shape and the thickness of the film can be easily tuned and reproduced by controlling some experimental conditions, such as the deposition time, scan rate, the nature of the supporting electrolyte and the magnitude of the applied potential.[22] We propose the use of staircase and pulse potential electrochemical techniques as tools for the easy and selective integration of the catalytic material into the microfluidic fuel cell. In this sense, Au_xPd_y mixtures with different mass ratio were first synthesized on glassy carbon electrodes in order to determine the effect of metal content in the glucose electrooxidation reaction, and after that synthesize the best Au_xPd_y ratio on a metallized glass plate (Ti, Ni, Au, tri-

layer) for its use as anodic electrode array into a glucose membraneless microfluidic fuel cell GMMFC.

Experimental

Electrochemical synthesis of Au_xPd_y mixtures on glassy carbon electrodes

Au_xPd_y mixtures with different metal ratio were synthesized using three different electrochemical techniques: cyclic voltammetry as staircase technique, square wave voltammetry and second harmonic AC voltammetry as pulse potential techniques. Briefly, an electrolytic solution was made using 2 mM $HAuCl_4$ (Sigma-Aldrich, 98%) and 3 mM Na_2PdCl_4 (Sigma-Aldrich, 99%) as Au^{3+} and Pd^{2+} ions source and 0.5 M H_2SO_4 (J. T. Baker, 99.7%) as electrolyte. Glassy carbon plates (SPI Instruments®, 1.44 cm^2) were used as working electrodes. Hg/Hg_2SO_4 sat. K_2SO_4 was used as reference electrode and a Pt wire as the counter electrode. Experiments were done using a standard three-electrode electrochemical cell through an AutoLab PGSTAT-30 Potentiostat/Galvanostatat at 25°C. Au_xPd_y with the highest Au content ($Au_{60}Pd_{40}$) was electrochemically synthesized using cyclic voltammetry with a potential range from -0.68 to 1.3 V *vs.* NHE at 100 mV s^{-1} for 20 cycles. Pulse potential techniques were used to increase the Pd concentration. Square wave voltammetry was used at two potential ranges: the first was applied from 1 to -0.15 V ($Au_{50}Pd_{50}$) and the second potential range was from 0.78 to -0.15 V *vs*. NHE ($Au_{35}Pd_{65}$); frequency (10 Hz), amplitude (0.05 V) and cycles (20) were kept as constant for both syntheses. Finally, second harmonic AC voltammetry was used in order to increase the Pd content ($Au_{15}Pd_{85}$) due to the facility of this technique to produce dendritic Pd structures;[23] the initial potential and end potential were of 1 and -0.15 V *vs*. NHE, respectively. The frequency was maintained at 10 Hz. The amplitude was of 0.001 V rms, with a modulation and interval times of 2 and 4 s, respectively. This experiment was done only for one cycle.

Electrochemical synthesis of Au, Pd and Au_xPd_y catalysts on the anode side of the GMMFC

After evaluating the electrocatalytic properties of Au_xPd_y mixtures in glassy carbon electrodes and find the best metal proportion, it was proceeded to synthesise this mixture in the anode side of the glucose membraneless microfluidic fuel cell GMMFC. Furthermore, bare gold and palladium were synthesised for comparison purposes. The anode electrode consisted in glass slide plates covered with a Ti, Ni and Au, tri-layer (1 cm^2). The electrodes were also covered with a Vulcan carbon ink (Vulcan® XC72, Cabot) to avoid the gold effect (from the tri-layer) in all experiments (see Scheme 1). The Vulcan ink was set to the tri-layer by the spray technique using 3 mg of Vulcan dispersed in isopropyl alcohol and Nafion® with a ratio of 1 mg Vulcan:75 µL alcohol:15 µL Nafion.

Au nanoparticles were obtained using cyclic voltammetry technique for 20 cycles through an electrolytic solution of 2 mM $HAuCl_4$ (Sigma-Aldrich, 98%) and 0.5 M H_2SO_4 (99.7%, J. T. Baker) as electrolyte. Potentials between 0.283 to 1.383 V *vs*. NHE were applied with a scan rate of 100 mV s^{-1}. Pd nanoparticles were obtained using an electrolytic solution of 3 mM Na_2PdCl_4 (Sigma-Aldrich, 99%) also in 0.5 M H_2SO_4. The potential range was between -0.067 to 1.383 V *vs*. NHE at 100 mV s^{-1} for 20 cycles. All experiments were carried out in the presence of N_2 (99.999%, Infra) as inert atmosphere at 25°C.

Physicochemical characterization of Au, Pd and Au_xPd_y electrocatalysts

The metal content of Au_xPd_y mixtures synthesized on glassy carbon was obtained using the Bruker S2Picofox X-ray fluorescence (XRF) operated at 50 kV and 600 µA. The electrocatalysts synthesized on the anodic Ti, Ni, Au tri-layer were characterized by X-ray diffraction (XRD) using a Bruker D8 Advance diffractometer operated at 30 kV and 30 mA. A JEOL JSM-7401F field emission scanning electron microscope (FE-SEM) was used to investigate the particle size. The elemental analysis was investigated with a coupled OXFORD EDS analysis INCA-model.

Electrochemical characterization of Au, Pd and Au_xPd_y electrocatalysts

The presence of the electrocatalysts synthesized on glassy carbon and on the anode compartment of the GMMFC was verified by electrochemical experiments (with a standard three electrodes electrochemical cell) using cyclic voltammetry in 0.5 M H_2SO_4 aqueous solution at 50 mV s^{-1} scan rate for 10 cycles at 25°C. The metals electrodeposited on the anode side and on glassy carbon electrodes were used as working electrodes; Hg/Hg_2SO_4 saturated in K_2SO_4 was used as reference electrode and a Pt wire as counter-electrode. The electrocatalytic activity of Au_xPd_y mixtures were evaluated in terms of the 10 mM glucose electrooxidation (Reagent grade, Sigma-Aldrich) in 0.3 M KOH (88%, J. T. Baker) as electrolyte and the saturated calomel electrode as reference for 10 cycles. The scan rate and temperature were of 20 mV s^{-1} and 25°C, respectively.

Fabrication and testing setup of the microfluidic fuel cell

A detailed description on the fabrication can be found elsewhere.[24] Briefly, a glass slide (76×26 mm) was covered with Ti and Ni layers using metal sputtering deposition. Then, photolithography was carried out on the metallic surface to define the conductive area for a consequent Au electrodeposition, showing a final electrode area of 1 cm^2 with an electrode separation of 500 µm (Scheme 1A and 1B). The fluids flow through a poly-dimethylsiloxane (PDMS, Sylgard 184, Dow Corning Inc.) channel which was made by soft-lithography from a master (SU-8 photoresist pattern) to define the double "Y" shape of the microchannel resulting in dimensions of 2 mm wide, 75 µm high and 25 mm long (Scheme 1A).

Au (used as target sample) and Au_xPd_y electrocatalysts were used as anode electrocatalysts and commercial Pt (20wt%, E-TEK) was used as cathode electrocatalyst (Scheme 1B).

Commercial Pt was incorporated to the electrode substrate via ink painting employing the same procedure than that used for the Vulcan carbon. 10 mM D-(+)-glucose (Sigma-Aldrich) and oxygen (zero/UHP degree, Infra) were used as fuel and oxidant, respectively. Both glucose and oxygen were dissolved in separate reservoirs using 0.3 M KOH (78%, J. T. Baker) as electrolyte. The fuel was deaerated using N_2 (99.999%, Infra) for 1 h. Likewise, the cathode solution was oxygenated for 1 h. The pressure-driven flow rate was 25 µL min^{-1} and it was regulated using a syringe pump (Cole Parmer, single-syringe infusion pump, 115 VAC). Voltage and current measurements were monitored using a BioLogic VSP Potentiostat/Galvanostat. The current and power densities here reported were calculated according to the geometric area of the electrodes in the micro-channel (0.075 cm^2).

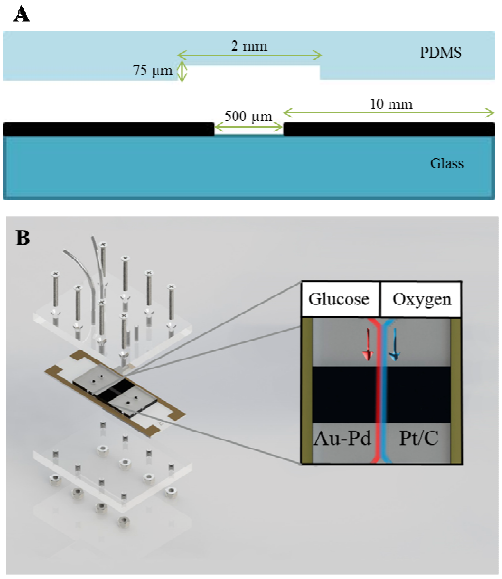

Scheme 1 A) PDMS channel and electrode dimensions, B) microfluidic cell design

Results and discussion

Electrochemical behaviour of Au_xPd_y with different metal ratio

The electrochemical response of Au_xPd_y materials in acidic medium (0.5 M H_2SO_4) is shown in Figure 1. The cyclic voltammograms were labelled according to the Pd mass content obtained by XRF (Table 1). Four well-defined regions were founded for the fourth compositions. The first region is attributed to the hydrogen adsorption/desorption region (0 to 0.3 V *vs*. NHE), the second region is related to the capacitive zone (0.3 to 0.6 V *vs*. NHE), the third regions to the formation and reduction of Pd oxides (0.6 to 0.9 V *vs*. NHE), and the fourth region is attributed to the formation of Au oxides and their respective reduction (0.9 to 1.7 V *vs*. NHE). The electrochemical profiles also showed an increase in the charge attributed to the hydrogen adsorption/desorption zone which is related to the higher content of Pd.

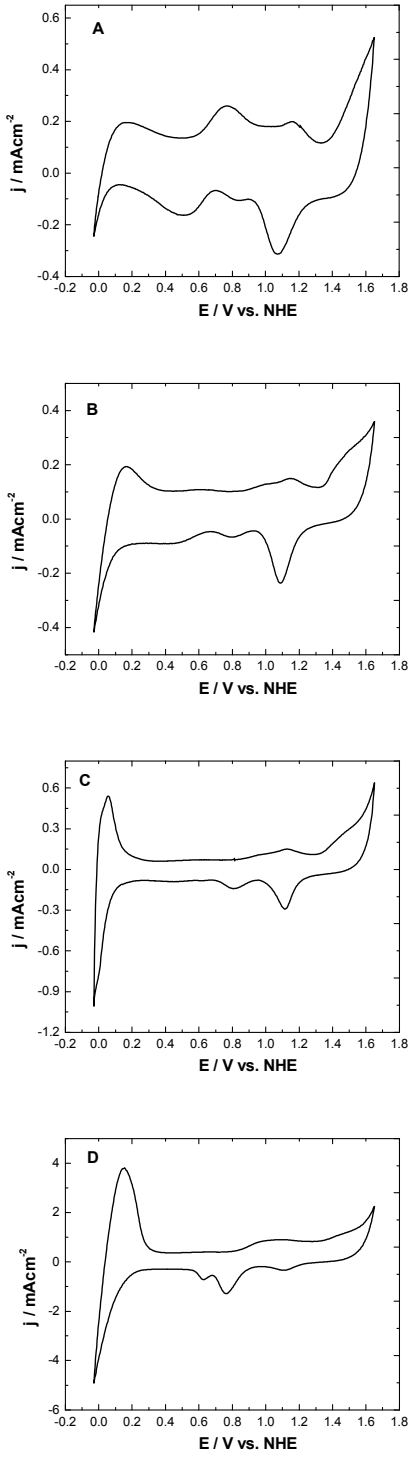

Figure 1 Cyclic voltammograms in saturated-N_2acidic medium of Au_xPd_y with different mass percentage: A) 60:40, B) 50:50, C) 35:65 and D) 15:85 on glassy carbon. Scan rate: 50 mV s^{-1}

Electrocatalytic activity of Au_xPd_y mixtures toward glucose oxidation

The electrocatalytic activity of the different Au_xPd_y mixtures was tested toward glucose electrooxidation reaction using 10

mM D-(+)-glucose (Sigma-Aldrich) and the results are shown in Figure 2.

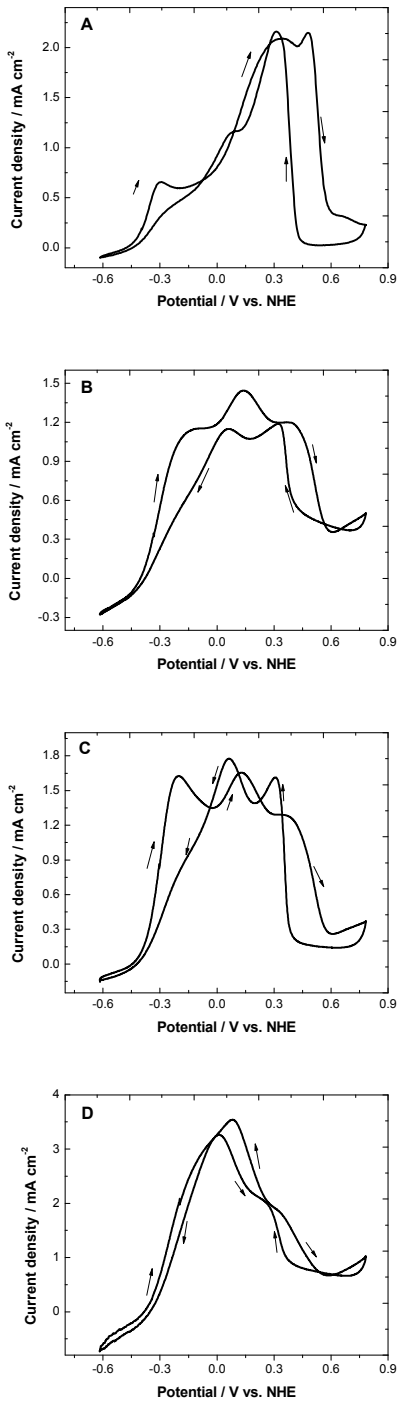

Fig. 2 Cyclic voltammograms in basic medium of Au_xPd_y with different mass content A) 60:40, B) 50:50, C) 35:65 and D) 15:85 for the glucose electrooxidation reaction using glassy carbon as substrate. Scan rate: 20 mV s^{-1}

As it is well known, Au is a good electrocatalyst for the glucose oxidation reaction.[12] In general, potential shifts towards more anodic values as function of palladium content were observed. The potentials for the first oxidation reaction were of -0.41, -0.35, -0.35 and 0.30 V *vs*. NHE for $Au_{60}Pd_{40}$, $Au_{50}Pd_{50}$, $Au_{35}Pd_{65}$ and $Au_{15}Pd_{85}$, respectively. This peak on Au surfaces is related to the first oxidation of glucose to gluconolactone.[25] On the other hand the onset potential for glucose oxidation reaction is associated with the potential value at which OH species are adsorbed on the metallic surface;[26] apparently the presence of Pd in the catalyst contributes to the formation of a higher quantity of M-OH sites.[27] This leads to remarkably high current densities for the $Au_{60}Pd_{40}$ and $Au_{50}Pd_{50}$ materials at lower potentials during the glucose oxidation process. In order to determine the best anode electrode for the microfluidic fuel cell we take into account the glucose oxidation potential value, the current density related with the fist oxidation process and the technique simplicity. In this sense, we decide to use the most common electrochemical technique: cyclic voltammetry which exhibited more negative potential than the others techniques.

Table 1 XRF analysis for the determination of mass content of AuPd mixtures

System	Au content / mass %	Pd content / mass %
AuPd A	59	41
AuPd B	48	52
AuPd C	36	64
AuPd D	15	85

Electrochemical synthesis of Au, Pd and Au_xPd_y on the anodic compartment of the GMMFC

$Au_{60}Pd_{40}$, Au and Pd were synthesised in the Ti-Ni-Au/Vulcan anodes. The electrochemical profiles of these materials are shown in Figure 3 (the behaviour for 1, 5, 10, 15, and 20 cycles are presented). In the three cases an increase of the current was observed due to a change in the conductivity of the electrode surface attributed to the formation of metallic Au, Pd and $Au_{60}Pd_{40}$ mixture or an increase in the surface area due to the formation of nanoparticles. For Au (Fig. 3-Au) the peak labelled as IV experiment a change in its peak potential between the first and the 20th cycle. In the first cycle the energy is required for the formation of nuclei and the crystal growth at the same time, which is higher than the succeeding cycles. As the number of cycles increase, the energy lowers because the consumed energy is mostly employed for the crystal growth. The same behaviour was observed for Pd (peak IV) and for $Au_{60}Pd_{40}$ (peak VIII for Pd and VII for Au). Returning to the case of Au, the peaks branded as I and II can be related to the formation of Au oxides, and the peak III to the reduction of the Au oxides.[28] In the case of Pd (Fig. 3-Pd), the peaks labelled as I, II, V, and VI are related to the hydrogen ad/desorption region. Meanwhile the peak III is related to the formation of PdHx,[29] and the peak IV to the reduction of Pd ions to metallic Pd.[30] As consequence, for $Au_{60}Pd_{40}$ mixture (Fig. 3 AuPd) peaks I, II, IX and X are associated to the Pd hydrogen ad/desorption region. The peaks labelled as III, IV and V corresponds to the formation of Pd oxides (peak III) and Au oxides (IV and V). Peak branded as VI corresponded to the

reduction of Au oxides, the labelled as VII to the formation of metallic Au and peak VIII to the formation of metallic Pd.

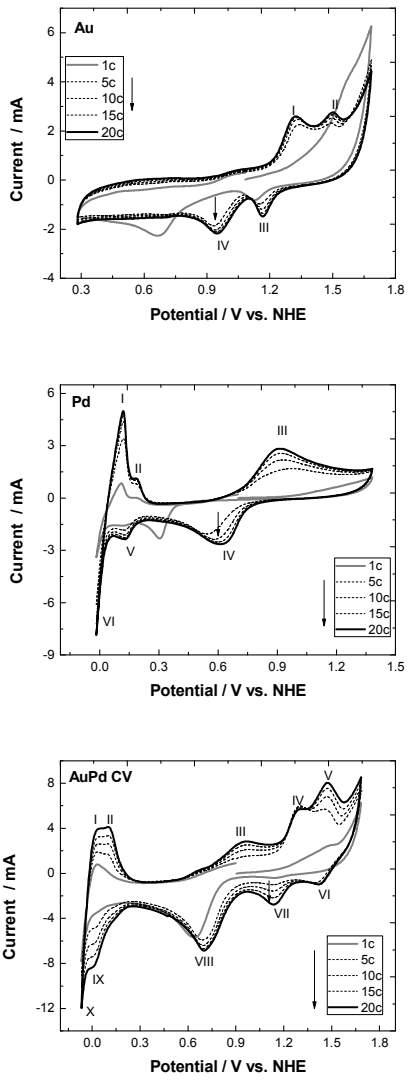

Fig. 3 Cyclic voltammograms for the electrochemical synthesis of Au, Pd and AuPd mixture on the anode compartment using Ti, Ni, Au tri-layer as substrate. Scan rate: 100 mV s^{-1}

Physicochemical characterization of Au, Pd and $Au_{60}Pd_{40}$ on the anodic compartment of the GMMFC

The XRD patterns for Au, Pd and $Au_{60}Pd_{40}$ using graphite as substrate are shown in Figure 4. Only some of the characteristic crystallographic planes of the different materials were identified due to the poor crystallinity than they exhibited. In the case of Pd, the peaks related to the (111) and (311) were located at 40.04 and 81.7°, respectively. Au exhibited the (111) and (220) planes, found at 38.24 and 64.72°. The $Au_{60}Pd_{40}$ mixture exhibited the (111) and (220) crystallographic planes which are characteristic of Au and Pd in their zero-valent form and were found at 39.15 and 66.3°, respectively. The graphite peaks were labelled in grey colour and correspond to the following peaks: (100), (101), (102), (004), (103), (110) and (112).

The (111) plane of the $Au_{60}Pd_{40}$ mixture was located between the characteristic degrees of the Au and Pd; which suggest changes in the internal structure of the mixture. In this sense, the lattice parameters were calculated from the (111) plane resulting in 3.83, 4.03 and 3.94 Å, for the Pd, Au and $Au_{60}Pd_{40}$ respectively, concluding that the internal distance between the crystallographic network for the $Au_{60}Pd_{40}$ is different than the Au and Pd. This behaviour is explained by Toda et al.[31] in terms of alloy formation. Additional experiments are needed to confirm the nature of the mixture in terms of interaction between both metals.

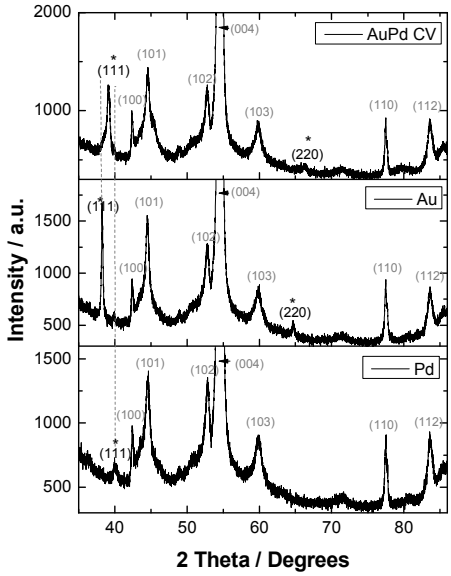

Fig. 4 X-ray diffraction patterns for Pd, Au and $Au_{60}Pd_{40}$ synthesized by cyclic voltammetry. The (111) is marked with a (*). The graphite peaks are marked in grey.

Approximation of the crystallite sizes was done applying the Scherrer's equation to the (111) plane resulting in sizes of 44, 16 and 33 nm for the Au, Pd and $Au_{60}Pd_{40}$ electrocatalysts, respectively. SEM images are illustrated in Figure 5 at two magnifications 10K and 50K X. All three cases showed uniform films, as can be observed at 10K X. Au film exhibited the existence of semi-spherical Au particles with low presence of aggregates (figure 5 at 50K X). The Pd films evidenced the existence of semi-spherical Pd particles with sharp-pointed growths. Finally, the $Au_{60}Pd_{40}$ mixture showed the presence of AuPd nanoflowers and the existence of semi-spherical particles. The particle shapes for the three materials can be related to the applied potential range.

Electrochemical characterization of Au, Pd and $Au_{60}Pd_{40}$electrocatalysts on the anodic compartment of the GMMFC

The electrochemical response of Au, Pd and $Au_{60}Pd_{40}$ in acidic medium (0.5 M H_2SO_4) is shown in Figure 6. In a potential range from 1.3 to 1.7 V *vs*. NHE (Fig. 6-Au) the formation of Au oxides is carried out, and at 1.16 V their respective reduction. For the case of Pd (Fig. 6-Pd), its three typical regions were observed, i.e. The hydrogen ad/desorption region in an potential interval from 0 to 0.3 V *vs*. NHE, the double layer region from 0.3 to 0.6 V, and finally the formation of Pd oxides and their respective reduction from 0.6 to 1.5 V *vs*. NHE. For the $Au_{60}Pd_{40}$ electrocatalyst a combination of the signals from the last two cases was observed. From 0 to 0.3 V the typical hydrogen ad/desorption region of Pd was exhibited. From 0.3 to 0.6 V, the double layer region was located. From 0.6 to 1 V occurs the formation of Pd oxides and from 1.3 to 1.5 V the formation of Au oxides took place. The reduction of Pd oxides was located at 0.6 V and the reduction of Au oxides at 1.1 V.

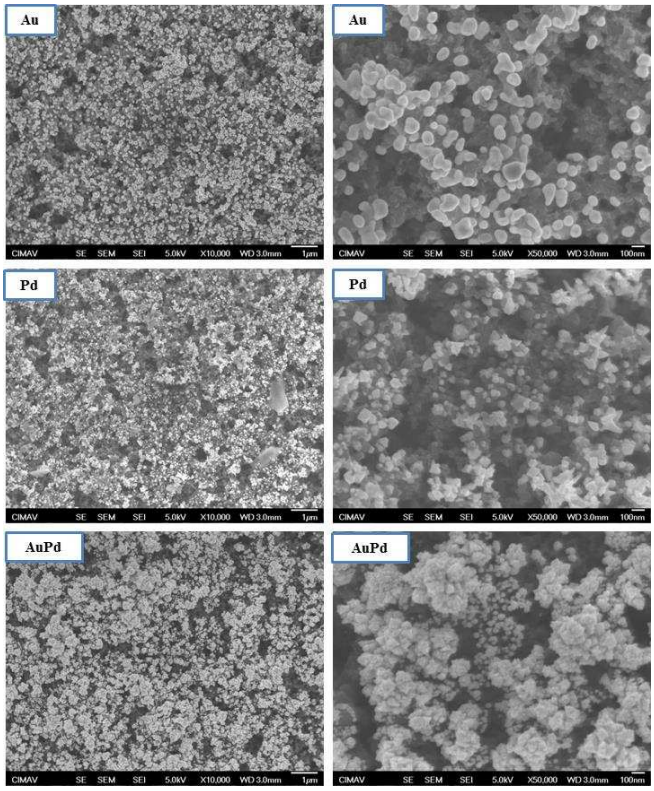

Fig. 5 FE-SEM micrographs for Au, Pd and $Au_{60}Pd_{40}$ synthesized by cyclic voltammetry (left, lower magnifications and right, higher magnification)

The electrochemically active surface area (ECSA) was calculated through the peak related to the reduction of the Au oxides (for Au and $Au_{60}Pd_{40}$ cases) and the hydrogen desorption region for the case of Pd using the theoretical values of 559 and 424 μC cm^{-2}, respectively.[32-33] The calculated values were of 6.98 (Au), 2.69 (Au in $Au_{60}Pd_{40}$ mixture) and 3.94 cm^2 (Pd).

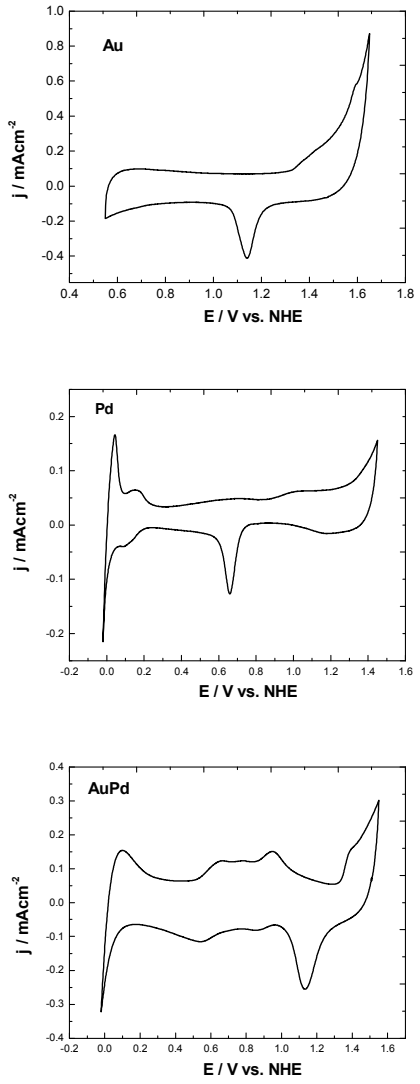

Fig. 6 Cyclic voltammograms in acidic medium of the electrical response of Au, Pd and $Au_{60}Pd_{40}$ synthesized by cyclic voltammetry using the tri-layer anode as substrate

The electrocatalytic activity toward 10 mM glucose electro-oxidation in 0.3 M KOH is shown in Figure 7-A. The Pd incorporation in the Au lattice modified the electrochemical behaviour for the glucose electrooxidation (black line) in which the successively glucose oxidations were shifted between Au and $Au_{60}Pd_{40}$ as can be observed in the figure 7-A. In the case of Au the interest reaction took place at -0.31 V *vs.* NHE. Meanwhile, for the $Au_{60}Pd_{40}$ electrocatalyst this reaction was carried out at -0.41 V vs. NHE. The current density for $Au_{60}Pd_{40}$ was 0.3 mA cm^{-2}.

Performance of the electrocatalysts in a glucose microfluidic fuel cell

Figure 7-B shows the polarization and power density curves for the microfluidic fuel cell operated with Au and $Au_{60}Pd_{40}$ as anode electrocatalysts in the presence of 10 mM glucose and Pt/V XC72 as cathode with O_2-saturated 0.3 M KOH. It is interesting to note that the open circuit potential in both cases show similar values, around 525 mV. The current density in the microfluidic fuel cell operated with $Au_{60}Pd_{40}$ as anode increased from 1.5 to 2.0 mA cm^{-2}. The power density (normalized by the geometrical area) of $Au_{60}Pd_{40}$ is slightly bigger than that obtained with Au/C as anode. These results remark the enhancement of electrocatalytic activity for the $Au_{60}Pd_{40}$ material.

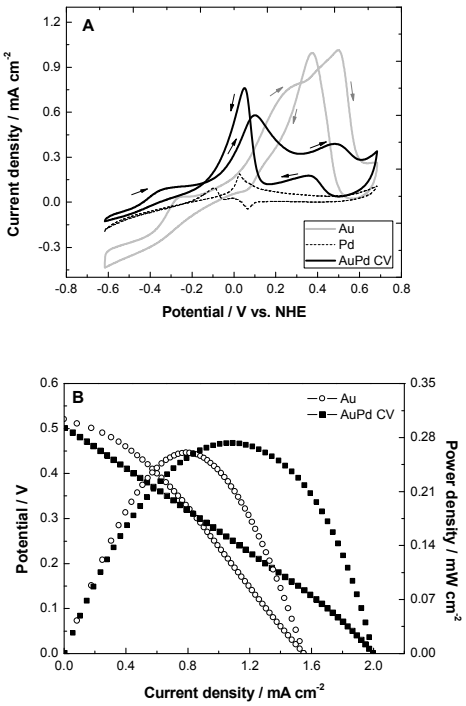

Fig. 7 A) Cyclic voltammograms of Au, Pd and $Au_{60}Pd_{40}$ toward 10 mM glucose electrooxidation reaction in 0.3 M KOH as electrolyte; scan rate: 20 mV s^{-1}. B) Polarization and power density curves in 10 mM glucose for the membraneless microfluidic fuel cells equipped with Au and $Au_{60}Pd_{40}$ anodes at 25 °C.

Conclusions

Pd content is critical in the electrocatalytic activity for the glucose electrooxidation reaction. In this work we explored its use as a bimetallic component in Au electrocatalysts. The glucose mechanism was affected by the bimetallic composition. Increasing the Pd content ($Au_{35}Pd_{65}$) the glucose mechanism started to exhibit similar current density for glucose and gluconolactone as a principal by-product, which means that both oxidations were carried out in almost 1:1 ratio. When the Pd metal concentration was much higher than Au ($Au_{15}Pd_{85}$) the peak related to the glucose and gluconolactone oxidation overlapped. At intermediate concentrations ($Au_{50}Pd_{50}$) Au showed higher effect than Pd which was observed in an increased of the current density toward gluconolactone oxidation due to the high content of (111) defects. The highest Au concentration was $Au_{60}Pd_{40}$ electrocatalyst which showed well-defined peaks related to both glucose and gluconolactone oxidations. This material also showed the most negative potential toward glucose oxidation. For this reason $Au_{60}Pd_{40}$ was electrodeposited in a glucose membraneless microfluidic fuel cell showing better performance than that obtained using a typical Au electrocatalyst as anode. In summary, AuPd materials showed high activity toward glucose electrooxidation reaction and can be easily electrochemically synthesized in the anodic compartment of membraneless microfluidic fuel cells avoiding the use of Nafion® as binder and hence decreasing the cell resistance.

Acknowledgements

The authors gratefully acknowledge the financial support of ANR-CONACYT 2011 (Grant 163114).

Notes and references

Corresponding author
[a] Centro de Investigación y DesarrolloTecnológico en Electroquímica, 76703 Querétaro, México. Phone: +52 442 2116069, Fax: +52 442 2116007. *E-mail: larriaga@cideteq.mx
[b] División de Investigación y Posgrado, Facultad de Ingeniería, Universidad Autónoma de Querétaro, 76010 Querétaro, México. Phone: +52 442 1921200 E. 65411, Fax: +52 442 1921200 E. 6006. +E-mail: janet.ledesma@uaq.mx
[c] Centro de Investigación en Materiales Avanzados, 31109 Chihuahua, México.
[d] Instituto de Microelectrónica de Barcelona, IMB-CNM (CSIC), Campus UAB, 08193 Bellaterra, Barcelona, España.

1. F. M. Cuevas-Muñiz, M. Guerra-Balcázar, J. P. Esquivel, N. Sabaté, L. G. Arriaga and J. Ledesma-García, *J. Power Sources*, 2012, **216**, 297-303.
2. S. Kerzenmacher, J. Ducrée, R. Zengerle and F. Von Stetten, *J. Power Sources*, 2008, **182**, 1-17.
3. A. Zebda, L. Renaud, M. Cretin, C. Innocent, F. Pichot, R. Ferrigno and S. Tingry, *J. Power Sources*, 2009, **193**, 602-606.
4. J. Ryu, H. S. Kimb, H. Thomas and D. Lashmore, *Biosens. Bioelectron.*, 2010, **25**, 1603-1608.
5. E. R. Choban, J. S. Spendelow, L. Gancs, A. Weickowski and P. J. A. Kenis, *Electrochim. Acta*, 2005, **50**, 5390-5398.
6. E. Kjeang, N. Djilali and D. Sinton, *J. Power Sources*, 2009, **186**, 353-369.
7. R. Galindo, A. Dector, L. G. Arriaga, S. Gutiérrez and P. Herrasti, *J. Electroanal. Chem.*, 2012, **671**, 38-43.
8. E. Katz and I. Willner, *J. Am. Chem. Soc.*, 2003, **125**, 6803-6813.
9. E. Katz, I. Willner and A. B. Kotlyar, *J. Electroanal. Chem.*, 1999, **479**, 64-68.
10. S. C. Wang, F. Yang, M. Silva, A. Zarow, Y. B. Wang and Z. Iqbal, *Electrochem. Commun.*, 2009, **11**, 34-37.
11. M. Guerra-Balcázar, F. M. Cuevas-Muñiz, F. Castaneda, R. Ortega, L. Alvarez-Contreras, J. Ledesma-García and L. G. Arriaga, *Electrochim. Acta*, 2011, **56**, 8758-8762.
12. M. Guerra-Balcázar, D. Morales-Acosta, F. Castaneda, J. Ledesma-García and L. G. Arriaga, *Electrochem. Commun.*, 2010, **12**, 864-867.

13. G. Zhang, Y. Wang, X. Wang, Y. Chen, Y. Zhou, Y. Tang, L. Lu, J. Bao and T. Lu, *Appl. Catal., B*, 2011, **102**, 614-619.
14. T. Hashishin and J. Tamaki, *Mater. Chem. Phys.*, 2008, **111**, 54-58.
15. D. Zhao, X. Chen, Y. Liu, C. Wu, R. Ma, Y. An and L. Shi, *J. Colloid Interface Sci.* , 2009, **331**, 104-112.
16. F. Yang, K. Cheng, T. Wu, Y. Zhang, J. Yin, G. Wang and D. Cao, *J. Power Sources*, 2013, **233**, 252-258.
17. M. Simoes, S. Baranton and C. Coutanceau, *Appl. Catal., B Environ.*, 2010, **93**, 354-362.
18. T. J. Schmidt, V. Stamenkovic, N. M. Markovic and P. N. Ross Jr, *Electrochim. Acta*, 2003, **48**, 3823-3828.
19. A. Abbaspour and F. Norouz-Sarvestani, *Int. J. Hydrogen Energy*, 2013, **38**, 1883-1891.
20. L. Yan, A. Brouzgou, Y. Meng, M. Xiao, P. Tsiakaras and S. Song, *Appl. Catal. B*, 2014, **150-151**, 268-274.
21. I.-S. Park, K.-S. Lee, S.-J. Yoo, Y.-H. Cho and Y.-E. Sung, *Electrochim. Acta*, 2010, **55**, 4339-4345.
22. N. Trombach, O. Hild, D. Schlettwein and D. Wöhrle, *J. Mater. Chem*., 2002, **12**, 879.
23. N. Arjona, M. Guerra-Balcázar, F. M. Cuevas-Muñiz, L. Álvarez-Conteras, J. Ledesma-García and L. G. Arriaga, *RSC Advances*, 2013, **3**, 15727.
24. A. Déctor, J. P. Esquivel, M. J. González, M. Guerra-Balcázar, J. Ledesma-García, N. Sabaté and L. G. Arriaga, *Electrochim. Acta*, 2013, **92**, 31.
25. N. Arjona, M. Guerra-Balcázar, G. Trejo, J. Ledesma-García and L. G. Arriaga, *New. J. Chem*., 2012, **36**, 2555.
26. A. Habrioux, K. Servat, T. Girardeau, P. Guérin, T. W. Napporn and K. B. Kokoh, *Curr. App. Phys*., 2011, **11**, 1149.
27. S. B. Aoun, Z. Dursun, T. Koga, G. S. Bang, T. Sotomura and I. Taniguchi, *J. Electroanal. Chem*., 2004, **567**, 175.
28. B. Lertanantawong, A. P. O'Mullane, W. Surareungchai, M. Somasundrum, L. D. Burke and A. M. Bond, *Langmuir*, 2008, **24**, 2856.
29. J. A. Abys and C. A. Dullaghan, *Electrodeposition of palladium and palladium alloys*. , John Wiley & Sons, New York, 2000.
30. T. R. Soreta, J. Strutwolf and C. K. O'Sullivan, *Langmuir*, 2007, **23**, 10823.
31. T. Toda, H. Igarashi, H. Uchida and M. Watanabe, *J. Electrochem. Soc*., 1999, **146**, 3750.
32. D. A. J. Rand and R. Woods, *J. Electroanal. Chem*., 1971, **31**, 29.
33. J. Tkac and J. J. Davis, *J. Electroanal. Chem*., 2008, **621**, 117.

